Article

Electron Spin Dynamics as a Probe of Molecular Dynamics: Temperature-Dependent Magnetic Field Effects on Charge Recombination within a Covalent Radical Ion Pair

Emily A. Weiss, Michael J. Tauber, Mark A. Ratner, and Michael R. Wasielewski

J. Am. Chem. Soc., **2005**, 127 (16), 6052-6061• DOI: 10.1021/ja043398y • Publication Date (Web): 05 April 2005

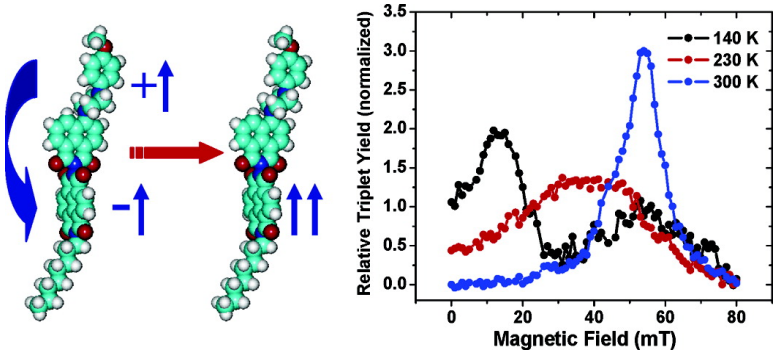

More About This Article

Additional resources and features associated with this article are available within the HTML version:

- Supporting Information
- Links to the 3 articles that cite this article, as of the time of this article download
- Access to high resolution figures
- Links to articles and content related to this article
- Copyright permission to reproduce figures and/or text from this article

View the Full Text HTML

J|A|C|S
ARTICLES
Published on Web 04/05/2005

Electron Spin Dynamics as a Probe of Molecular Dynamics: Temperature-Dependent Magnetic Field Effects on Charge Recombination within a Covalent Radical Ion Pair

Emily A. Weiss, Michael J. Tauber, Mark A. Ratner,* and Michael R. Wasielewski*

Contribution from the Center for Nanofabrication and Molecular Self-Assembly and Department of Chemistry, Northwestern University, Evanston, Illinois 60208-3113

Received November 1, 2004; E-mail: wasielew@chem.northwestern.edu

Abstract: The electron spin−spin exchange interaction, 2*J*, in radical pairs (RPs) is exquisitely sensitive to the details of molecular structure and can thus serve as an important probe of structural dynamics in RPs of potential interest to photonic and electronic devices. Photoinitiated ultrafast two-step charge separation produces ^{1}(MeOAn$^{+\bullet}$−6ANI−NI$^{-\bullet}$), where MeOAn = *p*-methoxyaniline, 6ANI = 4-(*N*-piperidinyl)-naphthalene-1,8-dicarboximide, and NI = naphthalene-1,8:4,5-bis(dicarboximide). Radical pair intersystem crossing subsequently produces ^{3}(MeOAn$^{+\bullet}$−6ANI−NI$^{-\bullet}$), and the total RP population decays with ∼10 ns lifetime at 140 K, which increases to nearly 30 ns at 300 K in toluene. The activation energy observed for this process is negative and can be explained by a mechanism involving a conformational preequilibrium of the RP followed by charge recombination. Over the same temperature range, the magnetic field effect (MFE) on yield of the triplet recombination product, MeOAn−6ANI−^{3*}NI, yields the magnitude of 2*J*, which directly monitors the superexchange electronic coupling for charge recombination. A single resonance in the MFE plot is observed at 300 K, which splits into two resonances at temperatures below 230 K, suggesting that there are two distinct groups of RP conformations at low temperature. The magnitude of 2*J* for the lower field resonance (10 mT) at 140 K is 5 times smaller than that of the high field resonance. At 300 K the equilibrium is shifted almost entirely to the set of conformers with the stronger electronic coupling. The motion that couples these two groups of conformations is the motion that most effectively gates the donor−acceptor electronic coupling.

Introduction

An observed electron-transfer rate within a complex system is almost always a mixture of rates through several different orbital pathways. The electronic coupling[1] and vibronic overlap,[2] which are very sensitive to molecular conformation and are also crucial determinants of long-distance electron-transfer rates, may vary widely from pathway to pathway. The process of identifying the contributions of several pathways to the overall electron-transfer process and determining the dependence of each on conformationally gated electronic coupling is experimentally challenging, but is fundamental to understanding electron transfer in molecules. This knowledge is critical if molecules are to act as electronic components within devices.

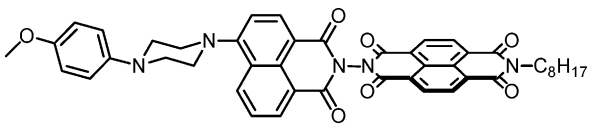

1

The covalent donor−chromophore−acceptor system, MeOAn−6ANI−NI, **1**, where MeOAn = *p*-methoxyaniline, 6ANI = 4-(*N*-piperidinyl)naphthalene-1,8-dicarboximide, and NI = naphthalene-1,8:4,5-bis(dicarboximide), and similar systems show nearly quantitative yields of electron transfer originating from the lowest excited singlet state of 6ANI. Many aspects of the photophysics of such systems have been characterized previously,[3−5] and the radical pair (RP) lifetimes are found to be tens to hundreds of nanoseconds. However, there are several complex aspects of the electron-transfer processes within **1**. First, the charge recombination process occurs through at least two pathways, one from the singlet-spin configuration of the RP to the singlet ground state, ^{1}(MeOAn$^{+\bullet}$−6ANI−NI$^{-\bullet}$) → MeOAn−6ANI−NI, and one from the triplet RP to an excited triplet state localized on the NI chromophore, ^{3}(MeOAn$^{+\bullet}$−6ANI−NI$^{-\bullet}$) → MeOAn−6ANI−^{3*}NI. It is difficult to distinguish the contributions of these two processes to the total recombination rate. Second, the recombination process slows with increasing temperature, so that traditional transition-state theory does not apply.[6] Finally, there is evidence to suggest that electron transfer

(1) Marcus, R. A.; Sutin, N. *Biochim. Biophys. Acta* **1985**, *811*, 265−322.
(2) Reimers, J. R.; Hush, N. S. *Chem. Phys.* **1990**, *146*, 105−114.
(3) Lukas, A. S.; Bushard, P. J.; Weiss, E. A.; Wasielewski, M. R. *J. Am. Chem. Soc.* **2003**, *125*, 3921−3930.
(4) Weiss, E. A.; Sinks, L. E.; Lukas, A. S.; Chernick, E. T.; Wasielewski, M. R. *J. Phys. Chem. B* **2004**, *108*, 10309−10316.
(5) Greenfield, S. R.; Svec, W. A.; Gosztola, D.; Wasielewski, M. R. *J. Am. Chem. Soc.* **1996**, *118*, 6767−6777.
(6) Closs, G. L.; Miller, J. R. *Science* **1988**, *240*, 440−447.

10.1021/ja043398y CCC: $30.25

within this molecule may be significantly influenced by molecular motions within the 6ANI chromophore.[7−9]

Superexchange and Magnetic Field Effects. The charge recombination process within **1** occurs via superexchange,[4] which is thought to be an important mechanism for efficient electron transfer within the photosynthetic reaction center,[10,11] and has been studied in various biomimetic systems.[12,13] The term was first used by Kramers[14] and later by Anderson[15,16] to describe the indirect exchange coupling of unpaired spins via filled orbitals which acquire paramagnetic character through mixing with charge-transfer excited-state configurations.[16] In the context of electron transfer, superexchange is the virtual mediation of charge transport from donor to acceptor via bridge orbitals electronically well separated from those of the donor and acceptor.

The rates of nonadiabatic electron-transfer reactions, k_{ET}, depend critically on the superexchange coupling, V_{DA}, whose magnitude gives the effective interaction energy between the relevant orbitals on the donor and acceptor.[17,18] When the charge-transport process originates from a state in which the redox centers are also paramagnetic, e.g. charge recombination from a RP, the superexchange coupling that dictates charge transfer (CT) from the RP to energetically proximate electronic states is the same coupling that determines the magnetic interaction between the unpaired spins of the RP.[6,14−16,19,20] Therefore, the magnitude of the magnetic interaction and its behavior mirrors that of V_{DA}.

The magnetic field effect (MFE) on the yield and rate of RP recombination directly reveals the magnitude of electron spin−spin exchange interaction between the spins within the RP, 2*J*, which is proportional to the square of the donor−acceptor superexchange coupling, V_{DA}.[21−24] The mechanistic details of the radical pair-intersystem crossing mechanism (RP-ISC) and the theory behind the MFE have been researched extensively[25−28] and applied to many donor−acceptor systems[3,21,29−35] including biological[36−40] systems. Following charge separation, the RP, initially formed in its singlet configuration, undergoes electron−nuclear hyperfine coupling-induced RP-ISC to produce the triplet RP. The subsequent charge recombination process is spin selective, i.e. the singlet RP recombines to the singlet ground state and the triplet RP recombines to yield the neutral local triplet MeOAn−6ANI−^{3}*NI. Application of a static magnetic field splits the RP triplet levels, and variation of the field strength modulates the efficiency of the ISC by adjusting the energies of triplet sublevels relative to that of the singlet level. When the Zeeman splitting of the triplet RP levels equals the intrinsic singlet−triplet splitting, 2*J*, of the RP, there is an increase in intersystem crossing rate. This increase translates into a maximum in triplet RP production and therefore a maximum in local triplet production upon recombination. By monitoring the yield of local triplet production as a function of applied magnetic field, 2*J*—the magnitude of the magnetic superexchange interaction[41,42]—can be measured directly.

In this work, the radical pair recombination rate and the yield of MeOAn−6ANI−^{3}*NI triplet product are found to depend dramatically on both magnetic field strength and temperature over a wide (>150 K) temperature range. Notably, in the MFE on triplet yield, we observe two distinct resonances below 230 K, which correspond to two sets of molecular conformations of the RP. We analyze the temperature dependence of the position and line shape of the 2*J* resonances to characterize the motion that interchanges these conformations in detail. Additionally, we determine the relative contributions of spin-selective pathways to the total recombination process using the magnetic field dependence of the RP recombination rate. This information allows us to analyze in depth the relative contributions of conformationally gated electronic coupling and of spin dynamics to the negatively activated charge recombination process within **1**.

Experimental Section

The synthesis and characterization of compound **1** has been reported previously.[33] Characterization was performed with a Varian 400 MHz NMR and a PE BioSystems MALDI-TOF mass spectrometer. Absorption measurements were made on a Shimadzu (UV-1601) spectrophotometer. The optical density of all samples was maintained between 0.3 and 1.0/cm at 420 nm, ($\epsilon_{6ANI,420nm} = 7000\ cm^{-1}\ M^{-1}$).[5] All samples were subjected to five freeze−pump−thaw degassing cycles.

For the nanosecond variable-temperature experiments, a liquid nitrogen-cooled optical Dewar (Janis Research VPS-100) was utilized. Each spectroscopic sample was loaded under nitrogen atmosphere into a sealed, homemade, ∼2−3 mm path length optical cell constructed from two transparent quartz windows and a Viton O-ring spacer. The sample holder was seated in the Dewar, which was then evacuated to $\sim 10^{-5}$ Torr. The sample temperature was maintained to within ±0.5 K by a Lake Shore Cryotronics model DRC-82C temperature controller.

(7) Sinks, L. E.; Wasielewski, M. R. *J. Phys. Chem. A* **2003**, *107*, 611−620.
(8) Saha, S.; Samanta, A. *J. Phys. Chem. A* **1998**, *102*, 7903−7912.
(9) Saha, S.; Samanta, A. *J. Phys. Chem. A* **2002**, *106*, 4763−4771.
(10) Marcus, R. A. *Chem. Phys. Lett.* **1987**, *133*, 471.
(11) Ogrodnik, A.; Michel-Beyerle, M.-E. *Z. Naturforsch.* **1989**, *44a*, 763.
(12) Kilsa, K.; Kajanus, J.; Macpherson, A. N.; Martensson, J.; Albisson, B. *J. Am. Chem. Soc.* **2001**, *123*, 3069−3080.
(13) Lukas, A. S.; Bushard, P. J.; Wasielewski, M. R. *J. Phys. Chem. A* **2002**, *106*, 2074−2082.
(14) Kramers, H. A. *Physica* **1934**, *1*.
(15) Anderson, P. W. *Phys. Rev.* **1950**, *79*, 350.
(16) Anderson, P. W. *Phys. Rev.* **1959**, *115*, 2.
(17) Marcus, R. A. *J. Chem. Phys.* **1965**, *43*, 679−701.
(18) Jortner, J. *J. Chem. Phys.* **1976**, *64*, 4860−4867.
(19) Yamashita, J.; Kondo, J. *Phys. Rev.* **1958**, *109*, 730.
(20) Feher, G.; Okamura, M. Y. In *Tunneling Conference*; Chance, B., Devault, D., Frauenfelder, H., Marcus, R. A., Schreiffer, J. R., Sutin, N., Eds.; Academic Press: New York, 1979; pp 729−743.
(21) Weiss, E. A.; Ahrens, M. J.; Sinks, L. E.; Gusev, A. V.; Ratner, M. A.; Wasielewski, M. R. *J. Am. Chem. Soc.* **2004**, *126*, 5577−5584.
(22) Kobori, Y.; Sekiguchi, S.; Akiyama, K.; Tero-Kubota, S. *J. Phys. Chem. A* **1999**, *103*, 5416−5425.
(23) Paddon-Row: M. N.; Shephard, M. J. *J. Phys. Chem. A* **2002**, *106*, 2935−2944.
(24) Volk, M.; Haberle, T.; Feick, R.; Ogrodnik, A.; Michel-Beyerle, M. E. *J. Phys. Chem.* **1993**, *97*, 9831−9836.
(25) Weller, A.; Staerk, H.; Treichel, R. *Faraday Discuss. Chem. Soc.* **1984**, *78*, 271−278.
(26) Hoff, A. J.; Gast, P.; van der Vos, R.; Vrieze, J.; Franken, E. M.; Lous, E. J. *Z. Phys. Chem.* **1993**, *180*, 175−192.
(27) Till, U.; Hore, P. J. *Mol. Phys.* **1997**, *90*, 289−296.
(28) Steiner, U. E.; Ulrich, T. *Chem. Rev.* **1989**, *89*, 51.
(29) Schulten, K.; Staerk, H.; Weller, A.; Werner, H.-J.; Nickel, B. *Z. Phys. Chem.* **1976**, *101*, 371−390.
(30) Tanimoto, Y.; Okada, N.; Itoh, M.; Iwai, K.; Sugioka, K.; Takemura, F.; Nakagaki, R.; Nagakura, S. *Chem. Phys. Lett.* **1987**, *136*, 42−46.
(31) Sakaguchi, Y.; Hayashi, H. *J. Phys. Chem. A* **1997**, *101*, 549−555.
(32) Werner, U.; Kuhnle, W.; Staerk, H. *J. Phys. Chem.* **1993**, *97*, 9280−9287.
(33) Weiss, E. A.; Ratner, M. A.; Wasielewski, M. R. *J. Phys. Chem. A* **2003**, *107*, 3639−3647.
(34) Tadjikov, B.; Smirnov, S. *Phys. Chem. Chem. Phys.* **2001**, *3*, 204−212.
(35) Tsentalovich, Y. P.; Morozova, O. B.; Avdievich, N. I.; Ananchenko, G. S.; Yurkovskaya, A. V.; Ball, J. D.; Forbes, M. D. E. *J. Phys. Chem. A* **1997**, *101*, 8809−8816.
(36) Blankenship, R. E.; Schaafsma, T. J.; Parson, W. W. *Biochim. Biophys. Acta* **1977**, *461*, 297−305.
(37) Michel-Beyerle, M. E.; Bixon, M.; Jortner, J. *Chem. Phys. Lett.* **1988**, *151*, 188−194.
(38) van der Vos, R.; Hoff, A. J. *Biochim. Biophys. Acta* **1995**, *1228*, 73−85.
(39) Werner, H.-J.; Schulten, K.; Weller, A. *Biochim. Biophys. Acta* **1978**, *502*, 255−268.
(40) Norris, J. R.; Bowman, M. K.; Budil, D. E.; Tang, J.; Wraight, C. A.; Closs, G. L. *Proc. Natl. Acad. Sci. U.S.A.* **1982**, *79*, 5532−5536.

The sample was allowed to equilibrate for 30 min at each temperature prior to photolysis.

The samples were excited with 5 ns, 1 mJ, 420 nm laser pulses focused to a 5-mm-diameter spot. The pulses were produced using the frequency-tripled output of a Continuum 8000 Nd:YAG laser which pumped a Continuum Panther OPO. The probe light was generated using a xenon flashlamp (EG&G Electrooptics FX-200) and detected using a photomultiplier tube (Hamamatsu R928) with high voltage applied to only 4 dynodes. The total instrument response time is 7 ns and is determined primarily by the laser pulse duration. Between 50 and 100 shots were averaged per kinetic trace with a LeCroy 9384 digital oscilloscope and sent to a microcomputer, which calculated the ΔA. Kinetic analyses were performed using a nonlinear least-squares fit to a general sum-of-exponentials using the Levenberg−Marquardt algorithm.

For the MFE experiment, the cryostat was placed between the poles of a Walker Scientific HV-4W electromagnet powered by a Walker Magnion HS-735 power supply. The field strength was measured by a Lakeshore 450 gaussmeter with a Hall effect probe. Both the electromagnet and the gaussmeter were interfaced with the data collection computer, allowing measurement and control of the magnetic field to $\pm 1 \times 10^{-5}$ T during data acquisition. Due to the length of the sample runs (>3 h) a small amount of sample degradation was observed, resulting in a decrease in the triplet yield at zero field, $\Delta A(B = 0)$, over the course of the experiments. To compensate for this, the magnetic field was reset to $B = 0$ mT every three kinetic traces and $\Delta A(B = 0)$ was plotted and fit with a polynomial or series of polynomials. These functions were used to calculate the relative triplet yield as a function of applied field strength. The relative triplet yield is thus:

$$\frac{T}{T_0} = \frac{\Delta A(B)}{\Delta A(B = 0)} \quad (1)$$

The results presented are an average of three or more experiments conducted on separate days with freshly prepared samples in spectrophotometric or freshly distilled ACS grade toluene.

Results

The 6ANI chromophore is oxidized at 1.2 V and reduced at −1.4 V vs SCE.[5] The oxidation potential of the MeOAn electron donor (0.79 V) is substantially less positive than that of 6ANI due to resonance stabilization of the aniline radical cation by the *p*-methoxy group. The reduction potential of NI is −0.5 V vs SCE.[43] The ground-state electronic spectrum of **1** in toluene exhibits a broad CT absorption centered near 400 nm due to the 6ANI chromophore, and a second band displaying vibronic structure at 343, 363, and 382 nm arising from a $\pi-\pi^*$ transition of the NI acceptor.

The RP, $MeOAn^{+\bullet}-6ANI-NI^{-\bullet}$, is produced by two sequential nonadiabatic electron-transfer reactions:

$$MeOAn-{}^{1*}6ANI-NI \xrightarrow{k_{CS1}} MeOAn-6ANI^{+\bullet}-NI^{-\bullet} \xrightarrow{k_{CS2}} MeOAn^{+\bullet}-6ANI-NI^{-\bullet}$$

where $k_{CS1} = 1.4 \times 10^{12}\ s^{-1}$ and $k_{CS2} = 1.0 \times 10^{11}\ s^{-1}$.[4] Figure 1 is a diagram of the electron-transfer processes that occur following photoexcitation. The free energy of the RP relative to the ground state for **1**, $E_{IP} = 1.97$ eV in toluene at room temperature, was calculated using the spectroscopic method

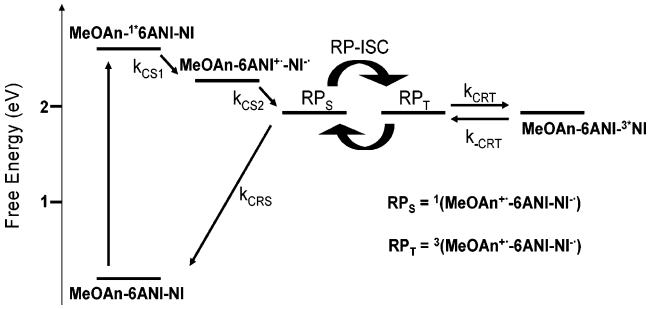

Figure 1. Diagram of charge-transfer processes following photoexcitation of MeOAn−6ANI−NI. k_{CS1} and k_{CS2} are the charge separation rates. RP_S and RP_T are the singlet and triplet radical pairs, which recombine with rate constants k_{CRS} and k_{CRT}, respectively.

outlined by Greenfield et al.,[5] which is based on Weller's dielectric continuum treatment for the energy of an RP in an arbitrary solvent. A complete list of the solvent reorganization energies calculated for the electron-transfer reactions in **1** using the Marcus formulation,[1] and internal reorganization energies, λ_I, calculated from DFT-energy minimized structures[44] of both the neutral and charged donors and acceptors can be found elsewhere.[4] The quantity relevant for our discussion is the total reorganization energy for charge recombination ($\lambda_I + \lambda_S = 0.54$ eV).

Temperature-Dependent Charge Recombination Kinetics. The room-temperature nanosecond transient absorption spectrum observed following 420-nm photoexcitation of **1** shows bands at 475 and 610 nm characteristic of the NI anion.[45] Nanosecond kinetic traces were obtained in toluene at 470, 475, and 605 nm at temperatures from 140 to 300 K. A representative transient kinetic trace at 475 nm can be found in Figure S1 (Supporting Information). The nanosecond kinetics display a single-exponential decay component followed by a residual low-amplitude absorption that decays on the microsecond time scale. Charge recombination rate constants were determined by a two-component exponential fit to the kinetic traces. The shorter, large-amplitude component marks the decay of $NI^{-\bullet}$, and therefore the recombination of the $MeOAn^{+\bullet}-6ANI-NI^{-\bullet}$ radical pair. The longer-lived, low-amplitude absorption is due to formation of an excited triplet state localized on NI, $^{3*}NI$, after charge recombination on the triplet surface.[4,33,46] At all temperatures and wavelengths, the zero-field amplitude of the slower component was <6%. We therefore report only the time constant of the major fast component in Table 1, and plot the corresponding rates as ln k_{CR} vs $1/T$ in Figure 2. From 160 to 260 K, the recombination time lengthens from 10 to 28 ns and exhibits plateaus at both ends of the temperature range.

The glass transition temperature of toluene is 117 K, and its melting point is 178 K.[47] The toluene solution remained optically clear throughout the temperature range except at 160 K. This temperature is close to a known critical temperature for toluene (153 K),[47] where the supercooled liquid still has low viscosity, but acquires some properties of a glass. At this temperature we find that the toluene crystallizes upon exposure to repeated laser

(41) Anderson, P. W. *Phys. Rev.* **1959**, *115*, 2−13.
(42) Shultz, D. A.; Fico, R. M.; Lee, H.; Kampf, J. W.; Kirschbaum, K.; Pinkerton, A. A.; Boyle, P. D. *J. Am. Chem. Soc.* **2003**, *125*, 15426−15432.
(43) Wiederrecht, G. P.; Niemczyk, M. P.; Svec, W. A.; Wasielewski, M. R. *J. Am. Chem. Soc.* **1996**, *118*, 81−88.
(44) Jaguar 3.5; Schrodinger, Inc., Portland, Oregon, 1998.
(45) Gosztola, D.; Niemczyk, M. P.; Svec, W.; Lukas, A. S.; Wasielewski, M. R. *J. Phys. Chem. A* **2000**, *104*, 6545−6551.
(46) Wiederrecht, G. P.; Svec, W. A.; Wasielewski, M. R.; Galili, T.; Levanon, H. *J. Am. Chem. Soc.* **2000**, *122*, 9715−9722.
(47) Wiedersich, J.; Surovtsev, N. V.; Rossler, E. *J. Chem. Phys.* **2000**, *113*, 1143−1153.

Table 1. Time Constants for Charge Recombination of the MeOAn$^{+\bullet}$−6ANI−NI$^{-\bullet}$ Radical Pair, Obtained from Fitting Kinetic Traces at 470, 475, and 605 nm (NI$^{-\bullet}$) as a Function of Temperature; MFE Plot Peak Position(s) in mT Obtained from Lorentzian Fits to the MFE Plots (Figure S2), except in the Coalescence Region, Where Peak Positions Were Estimated from the Plots in Figure 4; Corresponding Values in meV ($2J$(meV) = $g\beta B_{2J}$), and Equilibrium Constants (from Eq 2, Where $2J_a$ = 10.1 mT and $2J_b$ = 57.7 mT, above Coalescence and from the Relative Integrated Intensities of the Peaks below Coalescence)

T (K)	τ_{CR} (ns)	B_{2J1}(mT)	B_{2J2}(mT)	ΔB_{2J}(mT)	$\Delta 2J$(meV)	K_{eq}
140	10.3	10.1	57.7	47.6	0.0055	0.76
150	10.5	11.5	57.2	45.7	0.0053	0.82
160	10.8					
170	12.3	11.3	57.0	45.7	0.0053	0.89
180	12.9	18.0	55.7	37.7	0.0044	0.87
190	15.4	∼21	∼50	29	0.0034	
200	17.0	∼20	∼54	34	0.0039	
210	18.2	∼29	∼46	17	0.0020	
220	19.4	∼28	∼51	23	0.0027	
230	20.5	∼38				
240	21.2	42.6				2.0
250	22.4	45.4				2.6
260	26.3	46.4				3.1
270	28.0	48.0				3.8
280	26.3	49.9				5.1
293	27.8	55.4				19
300	26.3	55.6				19

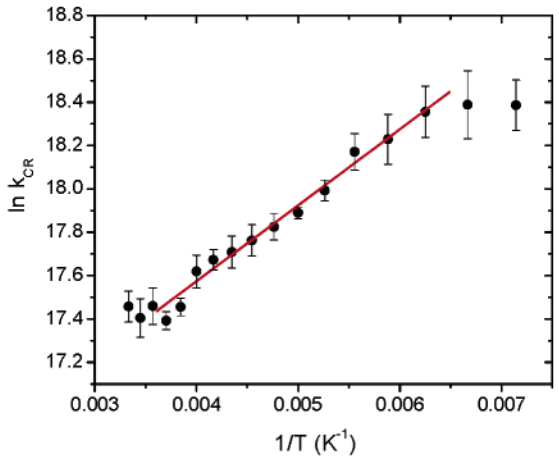

Figure 2. Charge recombination rate of the MeOAn$^{+\bullet}$−6ANI−N1$^{-\bullet}$ RP in toluene plotted vs inverse temperature for 140−300 K. The fit in the 160−260 K region (R^2 = 0.988) is to the equation $k_{obs} = A \exp(-x/T)$, where $A = 1.1 \times 10^7$ s^{-1} and $x = -0.03$ eV. Error bars are standard deviation of the decay rates measured at several wavelengths for multiple sample runs.

pulses, which causes the sample to scatter light, resulting in larger error bars for measurements close to that temperature.

Temperature-Dependent Magnetic Field Effects. Figure 3 shows selected plots of the relative yield of localized triplet recombination product versus applied magnetic field for temperatures from 140 to 300 K. The most obvious feature of Figure 3 is the dramatic increase in the size of the MFE as temperature is increased. The triplet yield is enhanced from its zero-field value to that at $B = 2J$ by a factor of 1.5 at 140 K and by a factor of 7.5 at 300 K.

The normalized MFE plots at each temperature, Figure 4, show a single, relatively narrow peak at 300 K ($2J$ = 55.2 mT) that broadens and shifts to lower field as the temperature is lowered. The coalescence temperature is ∼230 K. Upon further cooling, the band splits. The band at higher field retains its peak position ($2J$ = 49−53 mT) down to 140 K. The lower-field

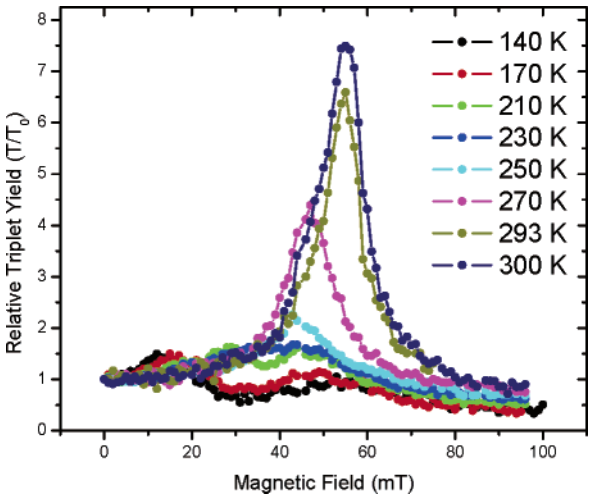

Figure 3. Relative triplet yield after charge recombination of **1** vs magnetic field strength for selected temperatures.

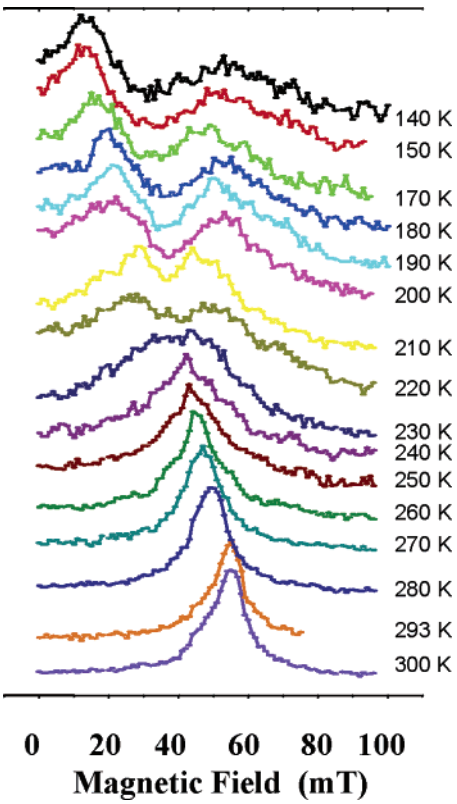

Figure 4. Triplet yield vs magnetic field plots from Figure 3 roughly normalized in amplitude so that positions of the $2J$ resonances along the magnetic field axis, Table 1, are highlighted.

band shifts continuously until it reaches 10.1 mT at 140 K. The two peaks at low temperature are due to two distinct sets of stable conformations of MeOAn$^{+\bullet}$−6ANI−NI$^{-\bullet}$, each of which has an average donor−acceptor coupling, V_{DA}, and therefore a distinct $2J$ resonance.

Discussion

The dataset obtained from the temperature dependence of the recombination rate and of the MFE allows for a multidimensional analysis of the charge recombination mechanism. Below, we will use the information provided by these data on the molecule's conformational dynamics and spin-selective recom-

bination pathways to discuss the negative activation of charge recombination within this system.

Throughout the following discussion, we assume that the temperature dependence of the position of the 2*J* resonance directly correlates with the temperature dependence of the square of the electronic coupling matrix element. Although the quantity 2*J* depends on both the electronic coupling and the difference in energy between the half-filled orbitals of the radical pair,[48,49] the temperature dependence of the one-electron orbital energies would rely almost exclusively on that of the solvent dielectric stabilization of the anion and cation. The experiment is performed in toluene, which has static dielectric constant of 2.67 at 177.5 K and of 2.44 at 298 K.[50] Using the Born continuum model for solvent stabilization energy, $E_{solv} = e^2/2r_i(1 - 1/\epsilon_s)$, the energy of a half-filled orbital would change by 0.06 eV for $r_i = 5$ Å[51] over this temperature range. Since the energies of the half-filled HOMO of MeOAn ($E \approx -0.8$ eV) and the half-filled LUMO of NI ($E \approx 0.53$ eV)[51] are approximately 10 times this value, the temperature-dependent orbital energy cannot account for the factor of 4 difference between the value of 2*J* at 140 K and that at 300 K. Additionally, any change in orbital energy due to the solvation effect would apply equally to both half-filled orbitals such that their energy difference would show no temperature dependence. Therefore, the assumption that 2*J* shifts due to the temperature dependence of the effective electronic coupling is a good one.

MFE Equilibrium Analysis. It is apparent from Figure 4 that, with increasing temperature, there is an increase in the intensity of the higher-field 2*J* resonance relative to that of the lower-field resonance at temperatures below the coalescence point and a shift in the average peak position of the resonance toward higher field above the coalescence point. The most likely explanation for this trend is the temperature dependence of the equilibrium constant for the conformational change. A similar argument has been put forth to explain temperature-dependent electronic coupling within C-shaped donor−acceptor molecules.[52] The interconversion of conformational groups a and b with average singlet−triplet splittings $2J_a$ and $2J_b$, leads to a temperature-dependent equilibrium constant, $K_{eq}(T)$, that, above coalescence, relates to their average signal, $2J_{avg}(T)$, as follows:[53]

$$K_{eq}(T) = \frac{(2J_a - 2J_{avg}(T))}{(2J_{avg}(T) - 2J_b)} \qquad (2)$$

Using this relationship above 230 K, where the single peak of these plots (Figure 4) corresponds to $2J_{avg}$ (Table 1), and the relative integrated intensities of the peaks for selected temperatures from 140 to 180 K (avoiding the coalescence region), we may determine the equilibrium constants for the conformational change over nearly the entire temperature region, Table 1. $2J_a$ and $2J_b$ in eq 2 are the peak positions at 140 K because these values are the best estimates for the resonances corresponding to the two relevant conformers in the slow-exchange regime. Qualitatively we observe that at the highest temperatures of our study (293 and 300 K) the equilibrium has shifted almost entirely to the *higher-field* set of conformations, i.e. that with strongest coupling between donor and acceptor. We note that shifts of 2*J* to higher fields with increased temperature have also been observed in flexibly bridged systems and have been attributed to a decrease in average radical pair distance with faster bridge motion.[54] However, in our study of **1**, the temperature dependence of the equilibrium constant is a much more satisfactory explanation because the bridge between the donor and the acceptor in **1** is significantly more rigid.

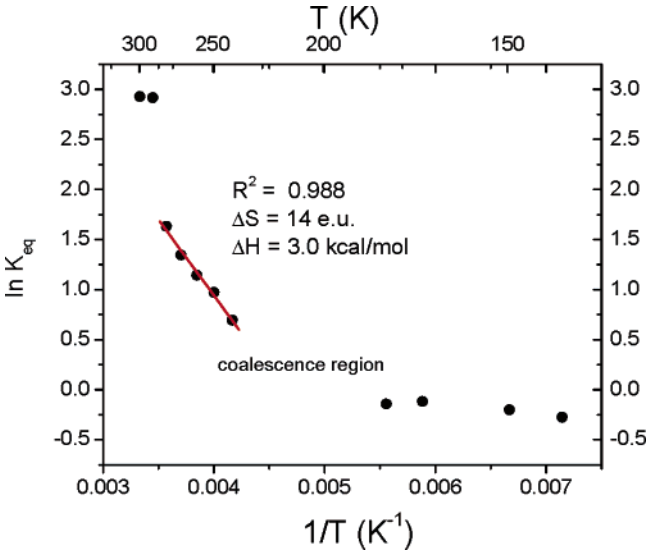

Figure 5. Plot of ln K_{eq} vs $1/T$ from 140 to 180 K and 240 to 300 K. Additional conformations contribute to the peak position above 280 K. The linear fit to the data from 240 to 280 K ($R^2 = 0.988$) yields an enthalpy difference of $\Delta H° = 3.0$ (±0.2) kcal/mol and an entropy difference of $\Delta S° = 14$ (±1) eu between the conformers. From 140 to 180 K, the equilibrium constant shifts very little.

A more quantitative approach to describing the conformational equilibrium observed in Figure 4 is a van't Hoff plot of ln K_{eq} vs $1/T$ from 140 to 300 K (excluding the coalescence region, for which it was difficult to integrate the individual peaks), Figure 5. A linear fit to the data of the van't Hoff plot from 240 to 280 K ($R^2 = 0.988$) yields an enthalpy difference of $\Delta H° = 3.0$ (± 0.2) kcal/mol and an entropy difference of $\Delta S° = 14$ (± 1) eu between the sets of conformers. Therefore, from 240 to 280 K, ΔG for the conformational change ranges from −0.3 to −0.9 kcal/mol, and the reaction from the lower-coupling set of conformers to the higher-coupling set of conformers is endothermic and entropically driven. It has been postulated previously that a positive entropy change may be induced by a greater exposure of a reactive site on the molecule to the solvent sphere, inducing reorganization—so-called "solvent entropy".[55,56] In this case, those reactive sites are the charges at each radical center.

It is evident from this plot that another higher-energy motion is contributing to the peak positions at 290 and 300 K. Excluding

(48) Weihe, H.; Gudel, H. U. *Inorg. Chem.* **1997**, *36*, 3632−3639.
(49) Kobori, Y.; Yago, T.; Akiyama, K.; Tero-Kubota, S.; Sato, H.; Hirata, F.; Norris, J. R., Jr. *J. Phys. Chem. B* **2004**, *108*, 10226−10240.
(50) Landolt, H. *Landolt-Börnstein physikalisch-chemische Tabellen*; Springer: Berlin, 1931.
(51) Greenfield, S. R.; Svec, W.; Gosztola, D.; Wasielewski, M. R. *J. Am. Chem. Soc.* **1996**, *118*, 6767−6777.
(52) Napper, A. M.; Read, I.; Waldeck, D. H.; Kaplan, R. W.; Zimmt, M. B. *J. Phys. Chem. A* **2002**, *106*, 4784−4793.
(53) Oki, M. *Applications of Dynamic NMR Spectroscopy to Organic Chemistry*; VCH: Deerfield Beach, Fl, 1985.
(54) Cao, H.; Fujiwara, Y.; Haino, T.; Fukazawa, Y.; Tung, C.-H.; Tanimoto, Y. *Bull. Chem. Soc. Jpn.* **1996**, *69*, 2801−2813.
(55) Battistuzzi, G.; Borsari, M.; Canters, G. W.; de Waal, E.; Leonardi, A.; Ranieri, A.; Sola, M. *Biochemistry* **2002**, *41*, 14293−14298.
(56) Gloss, L. M.; Matthews, C. R. *Biochemistry* **1998**, *37*, 16000−16010.

these outliers, this plot is clearly biphasic. From 140 to 180 K, the equilibrium constant changes very little, while from 240 to 280 K, the nature of the equilibrium between the two conformers is very different. We suspect that the discontinuity in the van't Hoff plot between the two temperature regions is due to the fact that the motion that couples the two resolvable conformers is itself coupled to many other motions in the system. If one of these enabling (or disabling) motions is activated in the 240−280 K range but not in the 140−180 K range, then the energetics of the equilibrium between conformers a and b will be considerably different from one region to another. In fact, as pointed out in previous work on the conformational gating of electronic coupling,[57] the energetic parameters extracted from the fit from 240 to 280 K may correspond to the *enabling* vibration or rotation and not to the motion that gates the electronic coupling.

MFE Line Shape Analysis. The superexchange coupling that dictates the value of 2*J* is defined at the relaxed geometry of the charge-separated state.[23] There are several effects that may contribute to the width of the 2*J* resonance. Lifetime or uncertainty broadening is small in this case, as the RP lasts at least 10 ns, which corresponds to a half-width of ∼1 mT. Spin−lattice relaxation (T_1) is also considered negligible for radical pairs in solution. Spin dephasing due to hyperfine interactions is, in the case of no molecular motion, the main source of line broadening. As calculated through the method of Weller,[58] with hyperfine coupling constants determined through line shape analysis of EPR spectra of the radical anion and cation, the total half-width due to the hyperfine interactions on both radical centers is ∼1.1 mT. The remaining homogeneous broadening is due to molecular motion leading to the stochastic modulation of the exchange energy.[59,60]

It is not surprising, then, that the spectra in Figure 4 in the fast-exchange regime fit well to Lorentzian line shapes (see, for example, Figure S2). In analogy to motional narrowing commonly observed in NMR and EPR spectra,[53,61] the MFE exhibits a narrowing of the resonances above 230 K around $2J_{avg}$, which results from the progressively shorter time spent in various configurations at higher temperatures. The narrow line limit in the MFE spectrum is ultimately determined by the magnitude of the hyperfine interactions and the extent of inhomogeneous broadening; however, this limit is not observed in the spectra presented in Figure 4. Instead, after the line shape narrows from 240 to 290 K, it then broadens again at 300 K, indicating (as do the outlying points at 290 and 300 K in the van't Hoff plot, Figure 5) that another higher-field conformation begins to contribute at this temperature.

An estimate of the lifetime of the molecule in two sets of conformations a and b can, in theory, be found by quantifying the Lorentzian fit to the spectra from 240 to 290 K.[62] However, this calculation requires that we know the intrinsic line width of the spectra in the absence of exchange, which is difficult to determine as the peaks below coalescence represent sets of conformations rather than a single conformer. We may more reliably estimate the rate of conformational interchange at coalescence, k_c, through the approximate expression[53]

$$k_c = \frac{\pi \Delta \nu_0}{\sqrt{2}} \tag{3}$$

where $\Delta\nu_0$ is the peak separation at 140 K. By eq 3, the rate of exchange needed for two peaks separated by ∼48 mT at 140 K to coalesce at 230 K is $k_c = 3.0 \times 10^9\ s^{-1}$ ($\tau_c = 1/k_c = 340$ ps).

By inspection of Figure 4, we can see that neither the low-field nor the high-field peak below 230 K broadens monotonically as the temperature increases as one would expect upon approaching coalescence. We believe, as has been noted consistently in this work, that this is because these peaks are themselves averages of several resonances and are therefore motionally narrowed by the fast exchange within each subset of conformers over this temperature range.

Magnetic Field Effects on the Recombination Rate. The observed charge recombination rate is a mixture of singlet and triplet components, k_{CRS} and k_{CRT}, respectively, which cannot be deconvoluted from the kinetic fits. To further investigate the temperature dependence of these spin-selective pathways, we studied the MFEs on the recombination rate as a function of temperature. Spin-selective recombination from the RP is field dependent since the applied magnetic field affects the percentage of the RP population that recombines via each of these pathways by modulating the RP-ISC. Figure 6 (black traces) shows the recombination rate as a function of field for selected temperatures. The red traces in this figure are simply the triplet yield plots from Figures 3 and 4 reproduced for comparison of the peak positions in the rate plot.

The recombination rate, even at its fastest at 140 K, is too slow to resolve any individual conformational groups and so the minima/maxima of the black traces shown in Figure 5 are always an average of the two triplet yield maxima, weighted by the equilibrium between the sets of conformations. Below 280 K, the overall recombination rate is minimized at the field at which maximum triplet is produced, $2J_{avg}$. At this field, the greatest percentage of the RP population is forced to recombine via the triplet pathway. This clearly shows that the singlet pathway is more efficient than the triplet pathway for $T < 280$ K: $k_{CRS} > k_{CRT}$. At 280 K, there is no field dependence of the rate, so $k_{CRT} \approx k_{CRS}$. Above 280 K, the rate is maximized at $2J_{avg}$, thus $k_{CRT} > k_{CRS}$. This trend accounts for the dramatic increase in the size of the field effect, Figure 3, from 140−300 K. As the yield of triplet recombination product is the observable in the MFE experiment, the sensitivity of the experiment to the magnetic field strength increases as the triplet pathway becomes more competitive with the singlet. This result implies that the singlet recombination process ($-\Delta G \approx 2$ eV) is negatively activated, while the triplet process ($\Delta G \approx 0$) becomes more efficient as temperature is increased.

What Motion Gates the Electronic Coupling? The conformational process evident in the temperature-dependent MFE data must be a motion that is energetically accessible and yields a significant change in geometry and distribution of unpaired spin. This motion will modulate orbital overlap and radical pair

(57) Davis, W. B.; Ratner, M. A.; Wasielewski, M. R. *J. Am. Chem. Soc.* **2001**, *123*, 7877−7886.
(58) Weller, A.; Nolting, F.; Staerk, H. *Chem. Phys. Lett.* **1983**, *96*, 24−27.
(59) Bittl, R.; Schulten, K. *J. Chem. Phys.* **1988**, *90*, 1794−1803.
(60) de Kanter, F. J. J.; den Hollander, J. A.; Huizer, A. H.; Kaptein, R. *Mol. Phys.* **1977**, *34*, 857−874.
(61) Pake, G. E.; Estle, T. L. *The Physical Principles of Electron Paramagnetic Resonance*; W. A. Benjamin, Inc.: Reading, MA, 1973.
(62) Weil, J. A.; Bolton, J. R.; Wertz, J. E. *Electron Paramagnetic Resonance. Elementary Theory and Practical Applications*; John Wiley and Sons: New York, 1994.

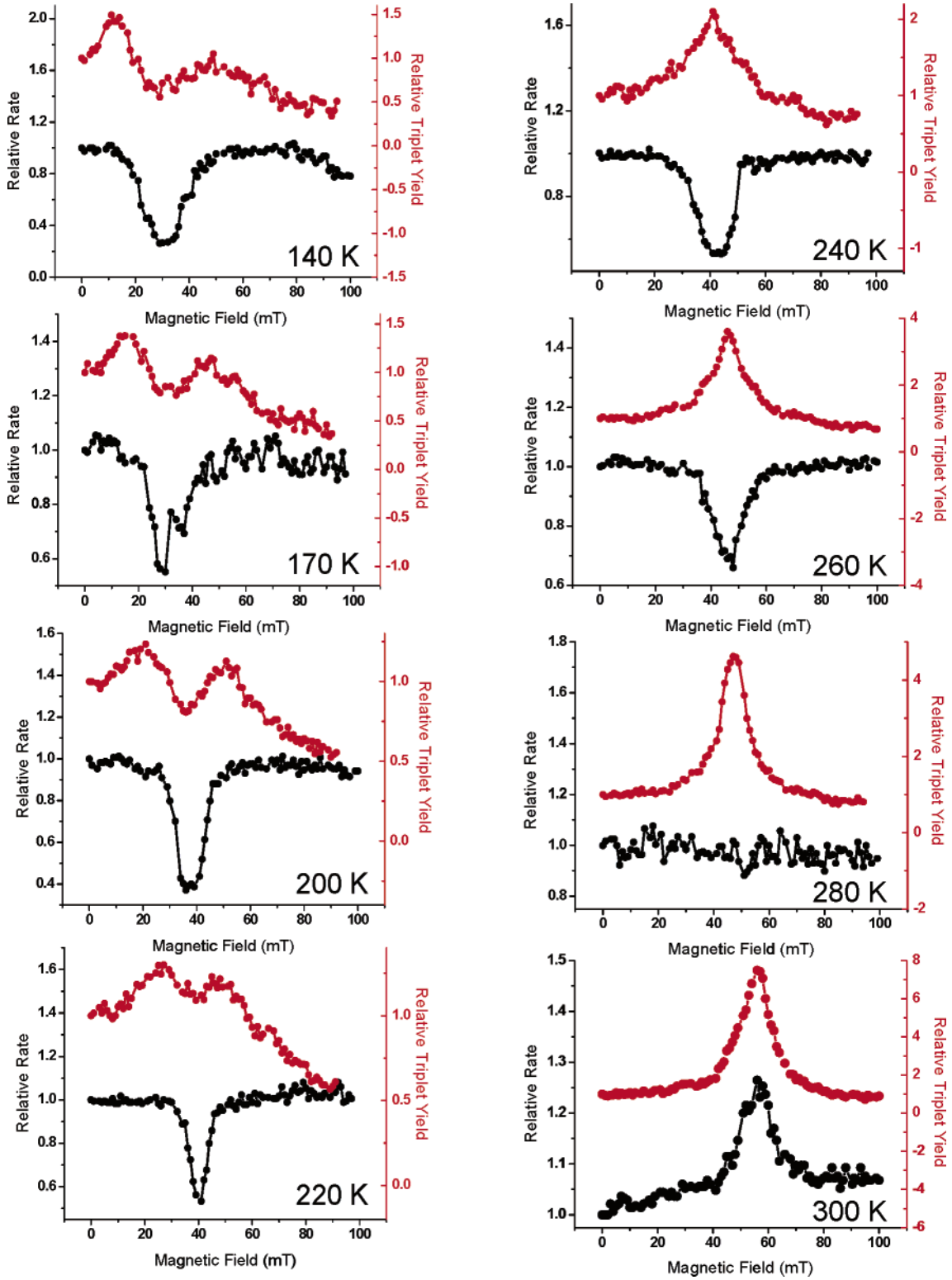

Figure 6. Plots of relative triplet yield (T/T_0) versus magnetic field (red) and recombination rate k_{CR}/k_{CR0} versus magnetic field (black) for selected temperatures. Triplet yield plots are identical to those in Figure 4.

distance and therefore gate the intramolecular electronic coupling. Within **1**, rotation around the N−N bond that links 6ANI and NI is severely restricted by steric hindrance between the imide oxygens on both 6ANI and NI.[4] For this reason we can eliminate this rotation as a significant contributor to the gating process. Coupled nitrogen inversion-ring torsion motion has been found to gate photophysical processes within many systems similar to 6ANI.[5,7−9,63−65] The piperazine nitrogens in the ground state of $MeOAn^{+\bullet}$−6ANI already have a significant amount of sp^2 character due both to the presence of the positive charge and to the very small dihedral angles between the nitrogen lone pairs and the p_z orbitals of the adjacent π systems, which facilitates conjugation between them. This geometry leads to a piperazine ring that is flattened relative to the neutral, unsub-

stituted chair configuration,[66,67] and thus nitrogen inversion is easier for the cation. There may also be chair-boat interconversion aided by the Coulombic interaction between ions (harpooning[33,68]). Finally, rotation of the methoxy group within $MeOAn^{+\bullet}-6ANI$ modulates the overlap between the lone pairs of the oxygen and the p_z orbitals of the phenyl carbons, which almost certainly affects the spin density distribution on the donor cation and therefore the effective radical pair distance. Clearly, the assignment of the motion that links the sets of conformations and therefore gates the electronic coupling is difficult for a system with many degrees of freedom and significant coupling between modes.

Mechanisms of Negative Activation. With the information gained through the MFE experiment about the conformational dynamics of the molecule in the RP state and the relative efficiencies of spin-selective recombination pathways, we are ready to discuss the possible mechanisms of negative activation of CR within MeOAn−6ANI−NI.

We may immediately eliminate the possibility put forth in a system previously studied in our group,[57] in which charge separation from a tetracene donor to a pyromellitimide acceptor via an oligo-*p*-phenylenevinylene bridge was negatively activated because high-temperature motions disrupted the conjugation between donor and acceptor and lowered the effective coupling. In our case, the MFE tells us that the donor−acceptor coupling increases significantly as the temperature is raised.

It is also possible to explain a negative activation barrier by postulating solvent mediation of the tunneling process, i.e. that the charge-transfer becomes somewhat adiabatic as the temperature is lowered and dynamic solvent effects become important.[7,69,70] This explanation requires that the longitudinal relaxation time of the solvent, τ_L, must be on the same order of magnitude as the time constant of the CT. The longitudinal relaxation time for a Debye solvent is proportional to the Debye relaxation time, τ_D:

$$\tau_L = \left(\frac{\epsilon_\infty}{\epsilon_s}\right)\tau_D, \quad \tau_D = \frac{4\pi\eta r^3}{k_B T} \tag{4}$$

where ϵ_∞ is the high-frequency dielectric constant (2.24), ϵ_s is the static dielectric constant, (which is a function of temperature[50]), η is the viscosity at a given temperature, and r is the effective radius of the tumbling solvent.[7,70,71] The longitudinal relaxation time of toluene was determined independently at 293 K[71] to be 4.76 ps, which implies a value of $r = 1.40$ Å. This solvent radius and the viscosities of toluene measured at temperatures ranging from ∼170 to ∼222 K[72] yield longitudinal relaxation times from eq 4 as listed in Table 2. At all temperatures, we note that the τ_L values determined by this method are at least 30-fold shorter than the recombination time measured experimentally at the corresponding temperature. Dynamic solvent control is therefore excluded as an explanation for the temperature dependence of the recombination rate.

Table 2. Toluene Viscosities, η,[72] and Longitudinal Relaxation Times, τ_L, Calculated from Eq 4, for Selected Temperatures

T (K)	η (poise)	τ_L (ns)	T (K)	η (poise)	τ_L (ns)
172	0.32	0.39	196	0.05	0.055
174	0.18	0.21	206	0.035	0.037
181	0.11	0.13	222	0.019	0.019
189	0.10	0.11			

In a near-barrierless reaction, the final electronic state surface crosses the initial state surface near its minimum, such that the lower-lying vibrational levels within the initial state are the most reactive levels. Thermal population of higher-lying vibrational states with increasing temperature decreases overlap with the final state, slowing the reaction. This explanation can also be excluded because a barrierless reaction requires that the magnitude of the driving force for recombination equals the reorganization energy for the recombination ($-\Delta G_{CR} = \lambda_{CR}$). Since we have established that the singlet pathway dominates the recombination throughout the negatively activated region, $-\Delta G_{CR} = \sim 2.0$ eV, and $\lambda_{CR} = 0.54$ eV, and the reaction cannot be barrierless.

The recombination process may also be negatively activated if charge recombination preferably or more efficiently comes out of the lower-coupling set of conformations, which is less populated at higher temperature. There are two possible reasons for this behavior. One is that recombination from the low-coupling conformer group is energetically favorable. Charge recombination via the singlet pathway is in the Marcus inverted region ($-\Delta G_{CR} > \lambda_{CR}$), such that an increase in the gap would only slow the reaction. As illustrated in the van't Hoff plot (Figure 5), $|\Delta G_{CR}|$ from the lower-coupling conformer group is greater than $|\Delta G_{CR}|$ from the higher-coupling conformer group (the reaction from lower- to higher-coupling conformer is spontaneous), so that there is no energetic reason for recombination from the lower-coupling conformer to be favored. Alternatively, since singlet and triplet recombination take place via different orbital pathways (singlet CR through the bridge LUMO and triplet CR through the bridge HOMO), it is conceivable that singlet CR can only occur from the low-coupling set of conformations and triplet CR only from the high-coupling set. Singlet CR is more efficient over the entire negatively activated region, so that, as temperature increases and the higher-coupling conformer is preferentially populated, the RP is increasingly forced to recombine via the slower triplet pathway, slowing the overall recombination rate. This would be a very reasonable explanation except for the fact that we know from the MFE on the recombination rate that it is not *just* the overall rate that is negatively activated; rather, the singlet rate itself becomes less efficient relative to the triplet rate as temperature increases. This can only happen if (1) the triplet pathway is positively activated and the singlet pathway is barrierless, an option we have already excluded or (2) the singlet pathway is itself negatively activated. Therefore, we must find an explanation that accounts for negative activation of a single-spin component of the overall rate.

(63) Okada, T. *Proc. Ind. Acad. Sci.* **1992**, *104*, 173−183.
(64) Mataga, N. *Acta Phys. Pol.* **1987**, *A71*, 767−776.
(65) Van der Auweraer, M.; Grabowski, Z., R.; Rettig, W. *J. Phys. Chem.* **1991**, *95*, 2083−2092.
(66) Lett, R. G.; Petrakis, L.; Ellis, A. F.; Jensen, R. K. *J. Phys. Chem.* **1970**, *74*, 2816−2822.
(67) Lambert, J. B.; Gosnell, J. L. J.; Elaine, S. D. *Rec. Chem. Prog.* **1971**, *32*, 119−132.
(68) Lauteslager, X. Y.; van Stokkum, I. H. M.; van Ramesdonk, H. J.; Brouwer, A. M.; Verhoeven, J. W. *J. Phys. Chem. A* **1999**, *103*, 653−659.
(69) Barbara, P. F.; Walker, G. C.; Smith, T. P. *Science* **1992**, *256*, 975−981.
(70) Heitele, H.; Michel-Beyerle, M. E.; Finckh, P. *Chem. Phys. Lett.* **1987**, *138*, 237−243.
(71) Harrison, R. J.; Pearce, B.; Beddard, G. S.; Cowan, J. A.; Sanders, J. K. M. *Chem. Phys.* **1987**, *116*, 429−448.
(72) Ngai, K. L.; Floudas, G.; Rizos, A. K. *J. Chem. Phys.* **1997**, *106*, 6957−6963.

The Preequilibrium Model. The existence of an equilibrium between distinct reactant states that precedes the reaction of one of those states to form product is known to account for an overall negative activation energy in a number of systems.[73−77] This kinetic scheme may also be applied in the present case, where we believe that one or several conformational equilibria between RP states conspire to allow charge recombination to take place. In this scheme, directly preceding charge recombination, there is a temperature-dependent equilibrium between two forms of the radical pair (not necessarily those resolved in Figure 4). The reaction, once the ion pair is formed, is then as follows:

$$\underset{\text{RP 1}}{\text{MeOAn}^{+\bullet}-\text{6ANI}-\text{NI}^{-\bullet}} \overset{k_1}{\underset{k_{-1}}{\rightleftharpoons}} \underset{\text{RP 2}}{\text{MeOAn}^{+\bullet}-\text{6ANI}-\text{NI}^{-\bullet}} \xrightarrow{k_2} \text{MeOAn}-\text{6ANI}-\text{NI}/\text{MeOAn}-\text{6ANI}-{}^{3*}\text{NI} \quad (5)$$

The steady state ($d[(MeOAn^{+\bullet} - NI^{-\bullet})]/dt = 0$) solution for the kinetics of this system gives a bimolecular rate constant for the formation of products, k_{obs}, equal to

$$k_{obs} = \frac{k_1 k_2}{k_{-1} + k_2} \quad (6)$$

We may then impose the preequilibrium condition: $k_2 \ll k_{-1}$,[77] which is very reasonable considering that k_{-1} is the rate of a molecular motion and k_2 is an electron transfer rate assumed to be on the nanosecond time scale. Then,

$$k_{obs} \approx \frac{k_1 k_2}{k_{-1}} \quad (7)$$

Expressing each rate constant in its Arrhenius form,

$$k_{obs} \approx \frac{k_1 k_2}{k_{-1}} = \frac{A_1 A_2}{A_{-1}} \exp[-(E_1 + E_2 - E_{-1})/k_B T] \quad (8)$$

where E_1 and A_1 are respectively the activation energy and the frequency factor for the process with rate k_1, etc. We then obtain

$$k_{obs} \approx \frac{A_1 A_2}{A_{-1}} \exp[-(\Delta G_{conf} + E_2)/k_B T] \quad (9)$$

where ΔG_{conf} is the free energy difference between the minima of the electronic surfaces of the charge-separated states RP 1 and RP 2, respectively. Now, if $\Delta G_{conf} < 0$, and $|\Delta G_{conf}| > E_2$, then the observed activation energy will be negative. Note that the conditions $\Delta G_{conf} < 0$ and $|\Delta G_{conf}| > E_2$ imply that $E_{-1} > E_2$. Therefore, for the initial condition $k_2 \ll k_{-1}$ to be observed, A_{-1} must be larger than A_2. This again is reasonable as A_{-1} is a frequency factor for a conformational change (usually assumed to be on the order of 10^{12} s^{-1}),[78] while A_2 corresponds to nonadiabatic CT and therefore must be proportional to the square of a transmission or tunneling coefficient from one electronic surface to another. We may then fit the negatively activated region (160 → 260 K) of a plot of k_{obs} vs inverse temperature to eq 9, Figure 2, to get $A_1A_2/A_{-1} = 1.1 \times 10^7$ s^{-1} and $\Delta G_{conf} + E_2 = -0.03$ eV.

In this scenario, the singlet recombination pathway includes the preequilibrium and is therefore negatively activated, while the triplet pathway displays the "traditional" Arrhenius behavior of an elementary reaction. Therefore, the singlet dominates at low temperatures, but the triplet becomes increasingly efficient until it is the dominant pathway above 280 K. These assignments fit well with the preequilibrium picture because the potential surface of the ground-state singlet recombination product will most likely cross the radical pair surface much closer to its minimum than will the near-degenerate triplet recombination product surface. Therefore, the singlet process is a much better candidate for the process given by rate k_2 in eq 5, which must have a fairly low activation energy E_2 such that $E_2 < E_{-1}$.

We note that RP 1 and RP 2 in eq 5 cannot be the two resolved in Figure 4, as the reaction intermediate, RP 2, never builds up significant population within the preequilibrium scheme. RP 1 and RP 2 are most likely conformers within the higher field set in Figure 4 that are coupled by a low-barrier motion.

Conclusions

The temperature dependence of the spin-selective charge recombination rate for the MeOAn−6ANI−NI radical pair in toluene has been investigated through transient absorption and MFEs on the rate itself and on the yield of triplet recombination product. The observed rate of charge recombination *increases* by a factor of 2.5 as the temperature is lowered from 300 to 140 K, while the average value of the donor−acceptor superexchange coupling, V_{DA}, *decreases* significantly over this range. Two distinct sets of conformations of the radical pair, with different values of V_{DA}, were identified through the temperature-dependent MFE measurement. The molecular motion that interchanges these two sets of conformations, which occurs at a rate of $\sim 3.0 \times 10^9$ s^{-1} at coalescence, therefore gates the electronic coupling. A plot of the equilibrium constant for the conformational change vs $1/T$ yielded $\Delta H = 3.0$ kcal/mol and $\Delta S = 14$ eu between the conformers (240−280 K), so that the reaction must be entropically driven in this temperature region. MFEs on charge recombination rate prove that the singlet recombination pathway dominates below 280 K, but its efficiency relative to the triplet pathway decreases as temperature increases.

A preequilibrium kinetic scheme is proposed to be the mechanism through which negative activation of the charge recombination can occur. This model fits well to the rate data and indicates that $\Delta G_{conf} + E_2$ (the driving force for the conformational change plus the activation energy for the charge recombination) is approximately −0.03 eV throughout the temperature range investigated. However, the conformations that participate in the equilibrium directly preceding charge recombination within this mechanism are not those that most influence the electronic coupling, as the reaction intermediate must never build up significant population, and therefore would not appear as resonances in the MFE plots. Detailed molecular dynamics studies on this system and on model compounds are necessary

(73) Kiselev, V. D.; Miller, J. R. *J. Am. Chem. Soc.* **1975**, *97*, 4036−4039.
(74) Zaman, K. M.; Yamamoto, S.; Nishimura, N. *J. Am. Chem. Soc.* **1994**, *116*, 12099−12100.
(75) Yamamoto, S.; Sakurai, T.; Yingjin, L.; Sueishi, Y. *Phys. Chem. Chem. Phys.* **1999**, *1*, 833−837.
(76) Fukuzumi, S.; Ohkubo, K.; Tokuda, Y.; Suenobu, T. *J. Am. Chem. Soc.* **2000**, *122*, 4286−4294.
(77) Frank, R.; Greiner, G.; Rau, H. *Phys. Chem. Chem. Phys.* **1999**, *1*, 3841−3490.
(78) Steinfeld, J. I.; Francisco, J. S.; Hase, W. L. *Chemical Kinetics and Dynamics*, 2nd ed.; Prentice Hall: Upper Saddle River, NJ, 1999.

in order to determine which conformations within this complex system are responsible for gating the donor−acceptor superexchange coupling and the charge recombination.

Acknowledgment. M.R.W. acknowledges support by the Division of Chemical Sciences, Office of Basic Energy Sciences, U.S. Department of Energy under Grant No. DE-FG02-99ER14999. M.A.R. acknowledges support from DARPA and the NSF Chemistry Division. E.A.W. thanks the Link Foundation and Northwestern University for fellowships. M.J.T. acknowledges the donors of the American Chemical Society Petroleum Research Fund for partial support of this research. We thank Dr. Boris Rybtchinski, Dr. Louise Sinks, and Dr. Igor Kurnikov for many helpful discussions, and Emilie Schierloh and Erin Chernick for synthetic assistance.

Supporting Information Available: Supplementary figures including a nanosecond kinetic trace and a representative fit of the MFE on triplet yield to a Lorentzian line shape. This material is available free of charge via the Internet at http://pubs.acs.org.

JA043398Y